PAPER • OPEN ACCESS

Intraband carrier dynamics in Landau-quantized multilayer epitaxial graphene

New Journal of Physics
The open access journal at the forefront of physics
Deutsche Physikalische Gesellschaft DPG | IOP Institute of Physics

Intraband carrier dynamics in Landau-quantized multilayer epitaxial graphene

Martin Mittendorff[1,2,8], Milan Orlita[3,4], Marek Potemski[3], Claire Berger[5,6], Walter A de Heer[5,7], Harald Schneider[1], Manfred Helm[1,2] and Stephan Winnerl[1]

[1] Helmholtz-Zentrum Dresden-Rossendorf, PO Box 510119, D-01314 Dresden, Germany
[2] Technische Universität Dresden, D-01062 Dresden, Germany
[3] Grenoble High Magnetic Field Laboratory, CNRS-UJF-UPS-INSA, F-38042 Grenoble, France
[4] Charles University Faculty of Mathematics and Physics, Ke Karlovu 5, 121 16 Praha, Czech Republic
[5] Georgia Institute of Technology, Atlanta, GA 30332, USA
[6] Institut Néel, Université Grenoble Alpes—CNRS, F-38042 Grenoble, France
[7] Department of Physics, King Abdulaziz University, Jeddah, Saudi Arabia
E-mail: Martin@Mittendorff.email and S.Winnerl@hzdr.de

Received 2 June 2014, revised 28 September 2014
Accepted for publication 4 November 2014
Published 8 December 2014

New Journal of Physics **16** (2014) 123021
doi:10.1088/1367-2630/16/12/123021

Abstract

We investigate the low-energy carrier dynamics in Landau quantized multilayer epitaxial graphene on $(000\bar{1})$ SiC, using 14 meV photons. The THz absorption is dominated by Landau-level transitions within the conduction bands of several graphene layers with different doping. Varying the magnetic field allows us to tune the THz-induced response from induced transmission around $B = 0$ to induced absorption at intermediate fields (1.5 T–3.3 T) and back to induced transmission at higher fields (3.3 T–7 T). The main features of this complex response are explained by a strong dependence of the absorption on the electron temperature. Furthermore a prolonged relaxation at high fields, which is attributed to reduced scattering via optical phonons, is observed.

Keywords: graphene, magnetic field, carrier dynamics

[8] Current address: Institute for Research in Electronics and Applied Physics, University of Maryland, College Park, Maryland 20742, USA.

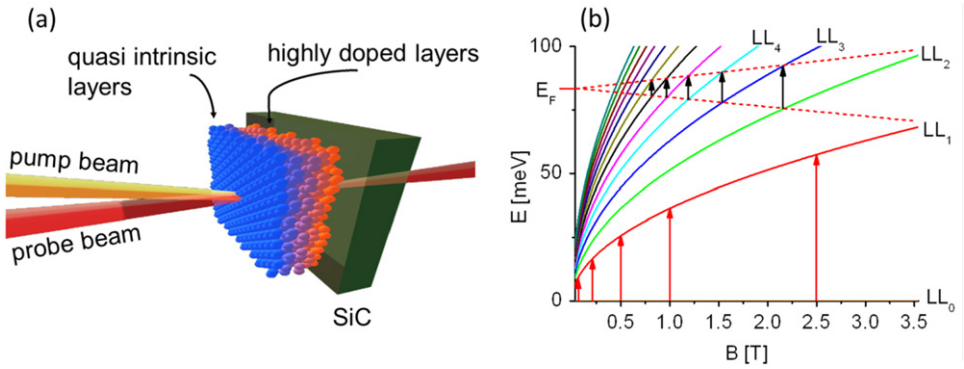

Figure 1. (a) Sketch of the sample with the differently doped graphene layers on SiC and the geometry of pump and probe beam. (b) Landau-level spectrum of graphene for positive energy, the negative part of the spectrum is symmetric. For Fermi energies differing from zero, intraband LL transition can be excited (indicated by black arrows). As the Fermi energy moves through the LLs with increasing magnetic field, the energy of the observable transition shifts linearly. For quasi intrinsic layers only interband transitions (indicated by red arrows) can be excited.

Applying a magnetic field to a graphene layer allows one to exploit the unique features of a non-equidistant Landau-level (LL) spectrum [1]. Many fascinating phenomena have been discovered in numerous transport experiments and continuous wave (cw) magneto-spectroscopy studies [2–8]. Recently strong influence of the Landau quantization on the carrier dynamics in graphene has been predicted by theory. In particular, resonant optical phonon scattering and carrier multiplication have been investigated [9–11]. Experimentally, however, the dynamics in Landau quantized graphene is largely unexplored, just one study has been carried out in the near-infrared spectral range [12]. That study reports increased relaxation times when *interband* transitions of a quasi-continuum of high-index LLs is probed. In contrast, our study investigates *intraband* LL transitions at 100 times smaller photon energies. Depending on the strength of the magnetic field, THz-induced transmission and absorption, respectively, is observed. This behaviour can be explained by the temperature dependence of the absorbance of highly doped interface layers, which is further corroborated by calculations via the Kubo formalism. At high fields the relaxation is slowed down as scattering via optical phonons is quenched.

The sample under investigation consists of roughly 50 layers of graphene grown by thermal decomposition on the carbon-terminated face of SiC [13]. Due to a rotation between the individual layers they are electronically decoupled and behave like single layers [14]. While the majority of layers are quasi-intrinsic, the layers at the interface to SiC are highly doped [15–17]. The free-electron laser (FEL) FELBE served as radiation source for degenerate pump–probe measurements. A sketch of the sample with the differently doped graphene layers and the pump–probe scheme is depicted in figure 1(a). The FEL provides a pulse train with a repetition rate of 13 MHz and linear polarization. While the photon energy was kept constant at 14 meV (wavelength: 88 μm) the magnetic field was varied from 0 T to 7 T. At the selected wavelength the pulse duration was around 10 ps, the pump pulse energy was 0.6 nJ (corresponding to a pump fluence of 0.3 μJ cm^{-2}). A magnet cryostat was used to apply the magnetic field in Faraday geometry and to keep the sample temperature at 10 K.

It is instructive to consider which LL transitions can be addressed in the multilayer graphene sample at THz frequencies. Only LL transitions where the absolute value of the LL

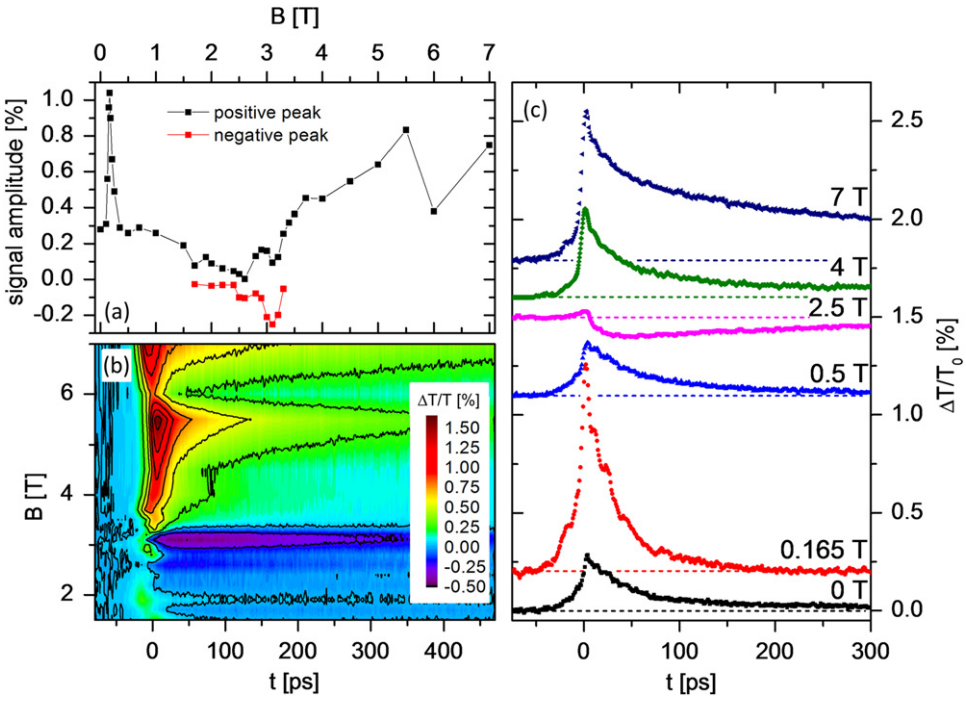

Figure 2. (a) Amplitude of the positive and negative pump–probe signal parts as a function of the magnetic field. (b) Map of the pump–probe signals between 1.5 T and 7 T, the pump induced change in transmission is colour coded. (c) Exemplary pump–probe transients at different magnetic fields. For a better visibility the curves are vertically shifted, the zero line is dotted for every measurement.

index is changed by ±1 are optically active [4]. Hence, in the quasi-intrinsic layers, featuring a partially filled zeroth LL, both of the energetically degenerate $LL_{-1} \Rightarrow LL_0$ and $LL_0 \Rightarrow LL_1$ transitions can be excited. In layers with an intermediate Fermi energy, where the zeroth LL is completely filled, still the upper transition ($LL_0 \Rightarrow LL_1$) can be excited, as long as LL_1 is only partly filled. The energy of these transitions scales with the square root of the magnetic field and becomes resonant with the photon energy of 14 meV for $B = 0.17$ T. In the doped layers with Fermi energies in the range of 100–400 meV a number of conduction-band LLs are completely filled. Hence, the only allowed THz transitions are between conduction-band LLs of successive index that are energetically located in the vicinity of the Fermi energy. Here the transition energy increases linearly with magnetic field (see figure 1(b)). Such cyclotron-like resonances have been observed in cw magneto-spectroscopy experiments on single layer graphene samples on the silicon-terminated face of SiC [18, 19].

The dependence of the THz induced transmission change on the magnetic field is depicted in figure 2. One striking feature is the strongly increased signal amplitude for $B \approx 0.17$ T (see figure 2(a)). This signal corresponds to resonant excitation of the transition $LL_{-1} \Rightarrow LL_0$ ($LL_0 \Rightarrow LL_1$) in the quasi-intrinsic layers. Upon resonance, the relaxation time decreases (see figure 2(c)). The origin of this fast decay is investigated in detail in a different study, where the energetically degenerate transitions $LL_{-1} \Rightarrow LL_0$ and $LL_0 \Rightarrow LL_1$ could be distinguished with circularly polarized radiation. Fast Auger scattering processes have been identified as the underlying mechanism for fast carrier redistribution [20]. Except for the $LL_{-1} \Rightarrow LL_0$ ($LL_0 \Rightarrow LL_1$) resonance, the observed THz-induced transmission changes are caused by carrier

redistributions within the highly doped layers. For magnetic fields in the range from 1.5 T to 3.3 T, a negative signal tail is observed subsequently to a short initial positive peak (see figures 2(a) and (b)). The positive peak almost vanishes for $B \approx 2.5$ T, indicating that in this field range induced absorption dominates over induced transmission. For magnetic fields above 3 T the signal amplitude exhibits a non-monotonic dependence on magnetic field with a general trend towards larger amplitudes at higher fields. Furthermore the relaxation times are longer as compared to the case of zero or smaller magnetic fields.

In order to understand the origin of the positive and negative signal parts for intermediate magnetic fields, we calculated the absorption of a stack of graphene layers based on the Kubo formalism as described in [4]. For the calculations we assume a hot Fermi distribution, which is valid after thermalization of the initial non-equilibrium distribution. The absorption of the sample is proportional to the real part of the dynamic conductivity $\sigma_{xx}^{(n)}(\omega)$. For each transition $\mathrm{LL}_{n-1} \Rightarrow \mathrm{LL}_n$ the dynamic conductivity can be calculated by

$$\sigma_{xx}^{(n)}\left(B, T_{\mathrm{el}}, \omega\right) = \frac{4\left(\frac{e \cdot B}{h}\right)e^2}{\omega} \cdot \frac{\mathrm{i}\frac{v_F^2}{p} \cdot \left(f\left(E_{n-1}, E_F, T_{\mathrm{el}}\right) - f\left(E_n, E_F, T_{\mathrm{el}}\right)\right)}{\left(E_n - E_{n-1}\right) - (\hbar\omega - \mathrm{i} \cdot \gamma)}, \tag{1}$$

where T_{el} is the electron temperature, $\gamma = 2$ meV accounts for collisional broadening, p is scaling the strength of the transitions ($p = 2$ for $n = 0$; $p = 4$ otherwise), and $f\left(E_n, E_F, T_{\mathrm{el}}\right)$ is the Fermi–Dirac distribution. The conductivity of the complete stack of graphene layers is obtained by adding up the conductivities of all layers characterized by their individual Fermi energies. The absorption at the photon energy of 14 meV is calculated by additionally summing over all relevant LL transitions.

In figure 3(a) the absorption is displayed in dependence of the magnetic field for different electron temperatures. For the calculation we assumed 30 layers of nearly intrinsic graphene with a Fermi energy of 5 meV , and four highly doped layers with Fermi energies of $E_{F1} \approx 380$ meV, $E_{F2} \approx 230$ meV, $E_{F3} \approx 150$ meV, and $E_{F4} \approx 80$ meV, respectively. Using these values as parameters, the absorption calculated with our simple model qualitatively resembles the main trend of the observed amplitude of the pump–probe signals (see figure 2(a)). For the four highly doped layers, the values used for the Fermi energies are very similar to the values reported for a graphene sample produced by the same growth method [17]. The calculated absorption shows a sharp maximum for $B = 0.17$ T corresponding to the $\mathrm{LL}_{-1,0} \Rightarrow \mathrm{LL}_{0,1}$ in the quasi-intrinsic layers. For higher fields a series of broad maxima and minima occurs (see figure 3(a)). The broad maxima correspond to cyclotron-like resonances in the doped layers, e.g. the maximum at 7.8 T corresponds to the first layer with $E_{F1} \approx 380$ meV and the maximum at 4.7 T to the second layer with $E_{F2} \approx 230$ meV. Even though the model assumes a fully thermalized carrier distribution, where all graphene layers exhibit the same electron temperature, it can explain the positive and negative pump–probe signals. The calculation reveals that an increase in electron temperature results in reduced absorption in the vicinity of the resonant field values (near 8 T and 4.5 T) and enhanced absorption otherwise (near 6 T and below 3 T). This effect, which is caused by an interplay of the smeared out Fermi edge with the B-field dependent filling of LLs, is responsible for the different signs observed in the pump–probe signals. Here the pump pulse heats the electronic system resulting in either induced transmission or induced absorption.

In contrast to the experiment, the modelled absorption exhibits more structure, especially for the low field part between 0.5 T and 4 T. In the experiment, due to the large spot size of the

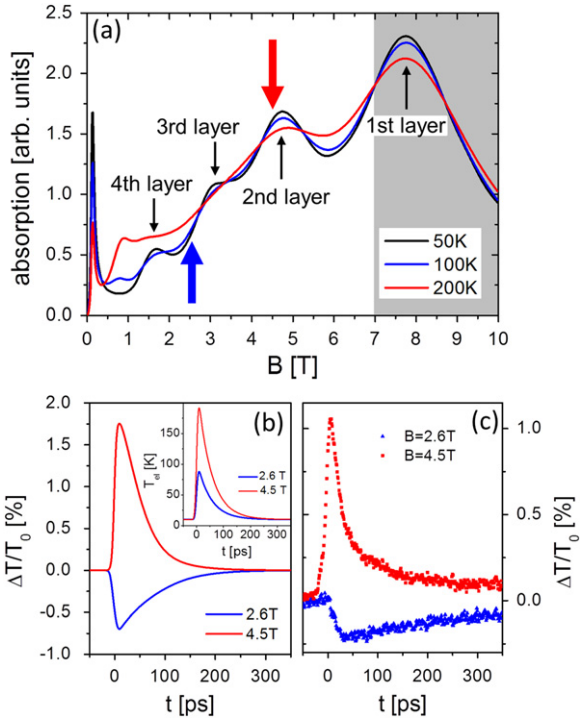

Figure 3. (a) Calculated absorption at a photon energy of 14 meV of the multilayer sample for different electron temperatures. The black arrows mark the layers that are responsible for the absorption maxima (at 50 K). The blue and red arrows indicate the magnetic-field values for which the pump–probe signals in part (b) are calculated. The grey shaded area was not accessible in our experiment. (b) Calculated pump–probe signals for a pump-induced increase of the electron temperature at two different magnetic fields. The electron temperatures are depicted in the inset. (c) Experimental pump–probe signals for the same magnetic fields as in the calculations in (b).

probe beam (~600 μm), areas with different Fermi energies are probed. As a result, the small features of the absorption get smeared out, in particular for the low field part where variations of the Fermi energy by few meV result in considerable changes in the absorption. In addition to the discussed n-type graphene layers at the interface to SiC multilayer epitaxial graphene can also feature p-type layers at the surface and also coupled graphene layers [21, 22]. The modelling of presumably small contributions from such layers is beyond the scope of our phenomenological approach.

In order to provide a more quantitative comparison between the model and the experiment, we calculate the pump-induced transmission change using the balance equation [23]

$$\frac{\mathrm{d}T_{\mathrm{el}}}{\mathrm{d}t} = \frac{P(t)}{c_p} - \frac{T_{\mathrm{el}} - T_{\mathrm{latt}}}{\tau}. \tag{2}$$

$P(t) = I(t) \cdot \sum_{\mathrm{layers}} \sum_n Re\left(\sigma_{xx}^{(n)}\left(T_{\mathrm{el}}, B\right)\right)/(\varepsilon_0 c)$ represents the absorbed power per unit area of the pump pulse (I: laser intensity, c: speed of light), c_p the specific heat and T_{latt} the temperature of the graphene lattice. The relaxation time τ is a phenomenological parameter. Furthermore, the transmission of the sample is calculated by

$$T\left(T_{\mathrm{el}}, B\right) \approx 1 - (1 - R) \cdot \sum_{\text{layers}} \sum_{n} Re\left(\sigma_{xx}^{(n)}\left(T_{\mathrm{el}}, B\right)\right)/(\varepsilon_0 c), \tag{3}$$

$R \approx 0.37$ accounts for reflections of the SiC substrate. The results for both the electron temperature and the induced transmission are depicted in figure 3(b). A good agreement between experiment and model is found for the magnetic field values 2.6 T and 4.5 T, where either purely positive or purely negative signals occur (see figures 3(b) and (c)). This is a strong indication that the observed positive and negative pump–probe signals are indeed related to intraband transitions in the doped graphene layers. However, the simple model cannot explain all features of the experimental dataset. In particular, the model predicts negative pump-signals for magnetic fields around 6 T, while in the experiment strongly reduced but still positive signals are observed. Such deviations are expected since the multilayer epitaxial graphene system is more complex than the simple model.

Before discussing the influence of the magnetic field on the carrier dynamics, we briefly review the well-researched carrier dynamics in graphene in the absence of a magnetic field. Photoexcited electrons in graphene quickly thermalize on a timescale of 100 fs via electron–electron interaction and scattering via optical phonons [24–26]. Subsequently the hot distribution cools on a timescale of a few picoseconds, mainly via optical phonons [25, 27]. Optical phonons decay into acoustic phonons on a similar timescale [28, 29]. This cooling dynamics results in a decay of the pump–probe signal on a timescale of few picoseconds in case the probe–photon energy is much larger than the optical phonon energy [24, 25, 30–32]. For probe–photon energies in the THz range and low lattice temperatures, however, much longer relaxation times of the order of a few 10 ps are observed as scattering via optical phonons is strongly suppressed [23, 33, 34]. Interestingly, microscopic theory reveals that scattering via optical phonons by electrons occupying the hot tail of the distribution is still the dominant contribution to the decay of the pump–probe signal, while acoustic phonons are responsible for even longer relaxation times in the range of 100 ps–1 ns [23, 35, 36]. Defects are assumed to considerably enhance acoustic phonon scattering via the supercollission mechanism [37, 38], resulting in ps relaxation times.

In accord with previous studies probing with probe–photon energies significantly below the optical phonon energy, long relaxation times on the 10 ps–100 ps scale are found in our experiment (see (figure 2(c)). To extract the decay time constants of the pump–probe signals we fitted the function

$$\Delta T\,(t)/T_0 = A \cdot \mathrm{erf}\,(t) \cdot \left(C \cdot \mathrm{e}^{\frac{-t}{\tau_1}} + \mathrm{e}^{\frac{-t}{\tau_2}}\right) \tag{4}$$

to the measured data. Here erf (t) is the error function that accounts for the excitation of the electrons, A and C are scaling factors for the amplitude of the signal and the ratio of the two exponential decays. The biexponential fit describes the experimental data well for all magnetic fields. For zero magnetic field the fit yields $\tau_1 = 43\,\mathrm{ps} \pm 5\,\mathrm{ps}$, $\tau_2 = 500\,\mathrm{ps} \pm 100\,\mathrm{ps}$. Referring to the discussion above, we suggest that τ_1 is related to the strongly quenched, but still relevant, cooling of the thermalized distribution via optical phonons, while τ_2 may be attributed to scattering via acoustic phonons, possibly mediated by defects. The dynamics of the $\mathrm{LL}_{-1} \Rightarrow \mathrm{LL}_0$ ($\mathrm{LL}_0 \Rightarrow \mathrm{LL}_1$) interband resonance occurring at $B = 0.17$ T is characterized by a fast initial decay. A detailed study of this resonance revealed that contributions of the non-thermalized carrier distribution influence the signal on a timescale of the order of 1 ps and that the fast decay is related to Auger scattering processes [20]. Induced transmission signals with a fast initial decay

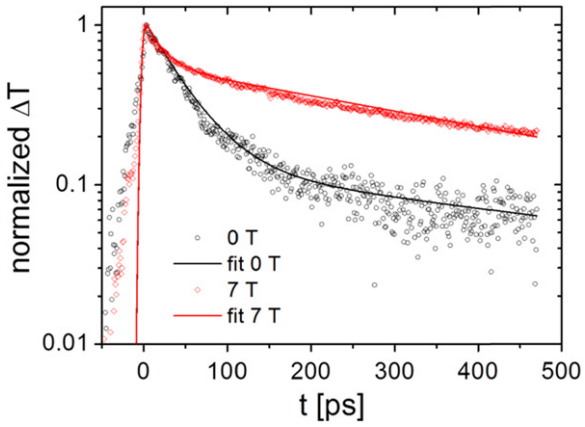

Figure 4. Pump–probe signals at 0 T and 7 T combined with the double exponential fit calculated by equation (4). The time constants are $\tau_1 = 43\,\text{ps} \pm 5\,\text{ps}$, $\tau_2 = 500\,\text{ps} \pm 100\,\text{ps}$ for $B = 0\,\text{T}$ and $\tau_1 = 20\,\text{ps} \pm 5\,\text{ps}$, $\tau_2 = 500\,\text{ps} \pm 100\,\text{ps}$ for $B = 7\,\text{T}$, respectively.

are also found for the higher magnetic fields, where the signals stem from intraband transitions within the doped layers (see figures 2(c) and 4). We speculate that Landau quantization, resulting in reduced phase space for carrier–carrier scattering and scattering via optical phonons, also in this case significantly prolongs the timescale of thermalization, similarly to the case of $LL_{-1} \Rightarrow LL_0$ ($LL_0 \Rightarrow LL_1$) interband resonance. Consequently, we attribute the initial peaks on a timescale of the pulse duration of 10 ps to signatures from the initial non-thermalized distribution and the subsequent fast decay to the attainment of a thermalized distribution. Following this argument, signals with initially positive peaks and negative tails (e.g. observed for $B = 2.5\,\text{T}$, see figure 2(c)) can be interpreted in the following way: the initial induced transmission is related to Pauli-blocking within the non-thermalized distribution, while the subsequent induced absorption is related to the response of the thermalized system. Scattering via optical phonons is expected to be strongly quenched by Landau quantization, unless the level separation is resonant with the optical phonon energy [9, 10]. The absence of a decay channel with a timescale of $43\,\text{ps} \pm 5\,\text{ps}$ in the pump–probe signals for high magnetic fields is consistent with the expected suppression of scattering via optical phonons. The missing contribution attributed to the optical phonons is the reason why the relaxation at longer delay times is much slower in the Landau quantized case as compared to the case of zero magnetic field (see figure 4). For the timescale attributed to acoustic phonons no significant change by Landau quantization is found.

A detailed understanding of both the electron–electron and electron–phonon related dynamics requires microscopic theory, which is beyond the scope of the present study. Note that the effects of Landau quantization on the carrier dynamics as discussed here, namely a reduction of both the rates for electron–electron and electron–optical phonon scattering, are in accord with the findings of Plochocka *et al* [12]. In that experiment, however, the values of the related scattering times are much shorter as 1.5 eV photons have been employed for pumping and probing.

In conclusion, our study reveals the THz response of Landau-quantized multilayer epitaxial graphene, which can be either induced transmission or induced absorption, depending on the value of the magnetic field. This behaviour is unambiguously explained by the dependence of strength of the involved intraband LL transitions on electron temperature.

Notably, these strong signals are caused by a small number of highly doped layers. The control of the THz response by the magnetic field together with the saturation properties of the system enables devices that can switch functionality from saturable absorption to saturable transmission. Finally, a phenomenological analysis of the carrier relaxation suggests that scattering via optical phonons and the thermalization via electron–electron scattering are strongly suppressed under Landau quantization.

Acknowledgments

We thank Peter Michel and the ELBE team for their dedicated support, as well as Ermin Malic, Florian Wendler, Torben Winzer and Andreas Knorr from the TU Berlin for stimulating discussions. Furthermore we acknowledge financial support via the Priority Programme 1459 Graphene from the German Science Foundation DFG (grant no. Wi3114/3). Part of this work has been supported by ERC-2012-AdG-320590 MOMB project, the EC Graphene Flagship, AFSOR and NSF (MRSEC—DMR 0820382). The research leading to these results has received funding from the European Community's Seventh Framework Programme (FP7/2007–2013) under grant agreement no. 226716.

References

[1] Goerbig M O 2011 *Rev. Mod. Phys.* **83** 1193
[2] Novoselov K S, Geim A K, Morozov S V, Jiang D, Katsnelson M I, Grigorieva I V, Dubonos S V and Firsov A A 2005 *Nature* **438** 197
[3] Bolotin K I, Ghahari F, Shulman M D, Stormer H L and Kim P 2009 *Nature* **462** 196
[4] Sadowski M L, Martinez G, Potemski M, Berger C and de Heer W A 2006 *Phys. Rev. Lett.* **97** 266405
[5] Orlita M *et al* 2008 *Phys. Rev. Lett.* **101** 267601
[6] Plochocka P, Faugeras C, Orlita M, Sadowski M L, Martinez G and Potemski M 2008 *Phys. Rev. Lett.* **100** 087401
[7] Crassee I, Levallois J, Walter A L, Ostler M, Bostwick A, Rotenberg E, Seyller T, van der Marel D and Kuzmenko A B 2011 *Nat. Phys.* **7** 48
[8] Booshehri L G *et al* 2012 *Phys. Rev.* B **85** 205407
[9] Wang Z-W, Liu L, Shi L, Gong X-J, Li W-P and Xu K 2013 *J. Phys. Soc. Japan* **82** 094606
[10] Wendler F, Knorr A and Malic E 2013 *Appl. Phys. Lett.* **103** 253117
[11] Wendler F, Knorr A and Malic E 2014 *Nat. Commun.* **5** 3703
[12] Plochocka P, Kossacki P, Golnik A, Kazimierczuk T, Berger C, de Heer W A and Potemski M 2009 *Phys. Rev.* B **80** 245415
[13] de Heer W A, Berger C, Ruan M, Sprinkle M, Li X, Hu Y, Zhang B, Hankinson J and Conrad E 2011 *Proc. Natl Acad. Sci. USA* **108** 16900
[14] Sprinkle M *et al* 2009 *Phys. Rev. Lett.* **103** 226803
[15] Berger C *et al* 2006 *Science* **3012** 1191
[16] Sun D, Wu Z-K, Divin C, Li X, Berger C, de Heer W A, First P N and Norris T B 2008 *Phys. Rev. Lett.* **101** 157402
[17] Sun D, Divin C, Berger C, de Heer W A, First P N and Norris T B 2010 *Phys. Rev. Lett.* **104** 136802
[18] Witowski A M, Orlita M, Stępniewski R, Wysmołek A, Baranowski J M, Strupiński W, Faugeras C, Martinez G and Potemski M 2010 *Phys. Rev.* B **82** 165305
[19] Orlita M, Crassee I, Faugeras C, Kuzmenko A B, Fromm F, Ostler M, Seyller T, Martinez G, Polini M and Potemski M 2012 *New J. Phys.* **14** 095008

[20] Mittendorff M *et al Nat. Phys.* (accepted) doi:10.1038/nphys3164
[21] Lin Y-M *et al* 2010 *Appl. Phys. Lett.* **97** 112107
[22] Ellis C T, Stier A V, Kim M-H, Tischler J G, Glaser E R, Myers-Ward R L, Tedesco J L, Eddy C R, Gaskill D K and Cernea J 2013 *Sci. Rep.* **3** 3143
[23] Winnerl S *et al* 2011 *Phys. Rev. Lett.* **107** 237401
[24] Breusing M, Ropers C and Elsaesser T 2009 *Phys. Rev. Lett.* **102** 086809
[25] Breusing M, Kuehn S, Winzer T, Malic E, Milde F, Severin N, Rabe J P, Ropers C, Knorr A and Elsaesser T 2011 *Phys. Rev.* B **83** 153410
[26] Mittendorff M, Winzer T, Malic E, Knorr A, Berger C, de Heer W A, Schneider H, Helm M and Winnerl S 2014 *Nano Lett.* **14** 105
[27] Malic E, Winzer T, Bobkin E and Knorr A 2011 *Phys. Rev.* B **84** 205406
[28] Yan H, Song D, Mak K F, Chatzakis I, Maultzsch J and Heinz T F 2009 *Phys. Rev.* B **80** 121403(R)
[29] Chatzakis I, Yan H, Song D, Berciaud S and Heinz T F 2009 *Phys. Rev.* B **83** 205411
[30] Dawlaty J M, Shivaraman S, Chandrashekhar M, Rana F and Spencer M G 2008 *Appl. Phys. Lett.* **92** 042116
[31] Obraztsov P A, Rybin M G, Tyurnina A V, Garnov S V, Obraztsova E D, Obraztsov A N and Svirko Y P 2011 *Nano Lett.* **11** 1540
[32] Plötzing T, Winzer T, Malic E, Neumaier D, Knorr A and Kurz H 2014 *Nano Lett.* **14** 5371
[33] George P A, Strait J, Dawlaty J, Shivaraman S, Chandrashekhar M, Rana F and Spencer M G 2008 *Nano Lett.* **8** 4248
[34] Strait J H, Wang H, Shivaraman S, Shields V, Spencer M and Rana F 2011 *Nano Lett.* **11** 4902
[35] Bistritzer R and McDonald A H 2009 *Phys. Rev. Lett.* **102** 206410
[36] Winnerl S *et al* 2013 *J. Phys.: Condens. Matter* **25** 054202
[37] Song J C W, Reizer M Y and Levitov L S 2012 *Phys. Rev. Lett.* **109** 106602
[38] Graham M W, Shi S-F, Ralph D C, Park J and McEuen P L 2013 *Nat. Phys.* **9** 103